An application of reliability-based robustness assessment of steel moment resisting frame structures under post-mainshock cascading events

Filipe L. A. Ribeiro [1]

André R. Barbosa [2]

and Luís C. Neves [3]

Abstract

The paper presented herein proposes a reliability-based framework for quantifying the structural robustness considering the occurrence of a major earthquake (mainshock) and subsequent cascading hazard events, such as aftershocks that are triggered by the mainshock. These events can significantly increase the probability of failure of buildings, especially for structures that are damaged during the mainshock.

The application of the proposed framework is exemplified through three numerical case studies. The case studies correspond to three SAC steel moment frame buildings of 3-, 9-, and 20- stories, which were designed to pre-Northridge codes and standards. Two-dimensional nonlinear finite element models of the buildings are developed using the Open System for Earthquake Engineering Simulation framework (OpenSees), using a finite-length plastic hinge beam model and a bilinear constitutive law with deterioration, and are subjected to multiple mainshock-aftershock seismic sequences.

For the three buildings analyzed herein, it is shown that the structural reliability under a single seismic event can be significantly different from that under a sequence of seismic events. The

[1]Ph.D. Student, UNIC, Department of Civil Engineering, Faculdade de Ciências e Tecnologia - Universidade Nova de Lisboa, Quinta da Torre, 2829-516 Caparica, Portugal, and Visiting Ph.D. Student, School of Civil and Construction Engineering, Oregon State University, Corvallis, USA, E-mail: f.ribeiro@fct.unl.pt

[2]Assistant Professor, School of Civil and Construction Engineering, Oregon State University, 220 Owen Hall, Corvallis, OR 97331-3212, USA, E-mail: andre.barbosa@oregonstate.edu

[3]Lecturer, Nottingham Transportation Engineering Centre, Faculty of Engineering, University of Nottingham, Nottingham NG7 2RD, England, UK; Assistant Professor, UNIC, Department of Civil Engineering, Faculdade de Ciências e Tecnologia - Universidade Nova de Lisboa, Quinta da Torre, 2829-516 Caparica, Portugal, E-mail:luis.neves@nottingham.ac.uk

reliability-based robustness indicator used shows that the structural robustness is influenced by the extent by which a structure can distribute damage.

Keywords: Aftershock, Nonlinear Dynamic Analysis, Robustness, Seismic Sequences.

INTRODUCTION

Structures in earthquake prone regions are susceptible to being damaged due to intense ground motion shaking. Traditionally, design and analysis of building structures only considers one single earthquake event, also known as a mainshock. However, in reality, structures can be subjected to cascading events, defined as events likely to be triggered by a major earthquake, such as aftershocks, fires, explosions, or tsunamis. The focus of this work is placed on sequences of ground motions that include the mainshock as well as aftershocks. Structural damage is typically observed in the large intensity mainshocks. Since the typical time interval between mainshocks and aftershocks is small, structural repair or retrofit is not possible and the mainshock-damaged structures are thus more susceptible to failure when an aftershock occurs. The term failure, as used herein, is synonymous with exceeding a defined limit state that may render structures unfit for use (Newmark and Rosenbleuth 1971).

In this paper, a measure of structural robustness is used to characterize the effect of aftershocks on the seismic safety of structures. With respect to aftershocks triggered by mainshocks, a structure is said to be more or less robust depending on its capacity to sustain post-mainshock damage without reaching failure. Three main approaches for quantifying structural robustness have been proposed in the literature. In the first approach, measures of structural robustness are derived from probabilistic risk assessments (Baker et al. 2008). Baker et al. (2008) defined a measure for quantifying structural robustness as a function of direct and indirect risk. Even though this approach is very powerful, the complexity and subjectiveness in the quantification of the direct and indirect risk in large structural systems hinders the application of this approach. In the second approach, measures of structural robustness are quantified in terms of ratios of structural properties (e.g. damage, energy, or stiffness) between undamaged and damaged structures (Starossek 2006; Cavaco et al. 2013). While these measures are useful in engineering practice, they fail to explicitly

describe failures. Finally, in the last approach, measures of structural robustness are defined as a function of the probabilities of failure of the intact and damaged structure. Examples of such measures are the indices presented by Frangopol and Curley (1987) and Lind (1995). It is worth noting that, as discussed in Starossek and Haberland (2008), both these measures evaluate structural redundancy rather than robustness. However, for buildings, redundancy is provided by the existence of alternative load paths which is the main mechanism providing robustness, rendering these indicators an adequate indirect measure of structural robustness. Robustness assessment of structures for cascading hazards is currently lacking in the literature.

There are two main challenges in modeling the effects of aftershock events on structures for computing structural robustness. The first challenge is related to the accurate modeling of expected mainshock-aftershock seismic sequences. This has been discussed extensively in (Ruiz-García 2012; Fragiacomo et al. 2004; Lee and Foutch 2004; Li and Ellingwood 2007; Luco et al. 2004; Luco et al. 2011; Ryu et al. 2011). Luco et al. (2011) and Ryu et al. (2011) performed mainshock-aftershock incremental dynamic analyses (IDA, Vamvatsikos and Cornell 2002) on single-degree-of-freedom models subjected to artificial sequences of mainshock-aftershock "back-to-back" structural analyses. The second challenge is related to accurate modeling of the effects of damage introduced by the mainshock on structural performance. To this effect, state-of-the-art modeling for estimation of structural performance/damage can be found in ATC-72 (PEER/ATC 2010). In the ATC-72 report emphasis is placed on phenomenological models that capture the main effects of strength and stiffness deterioration.

In this study, a probabilistic framework for the assessment of structural robustness under mainshock triggered aftershocks is developed. Emphasis is placed on the evaluation of the structural robustness as a function of the probability of failure (or the reliability index) under different damage scenarios. In the probabilistic methodology, nonlinear dynamic time-history analyses of structural computational models of buildings are used to estimate the recorded structural damage due to multiple mainshock-aftershock sequences. Mainshock and aftershock incremental dynamic analyses are carried out following the approach proposed by Ryu et al. (2011), where artificial mainshock-

aftershock sequences are used in the "back-to-back" nonlinear dynamic time-history analyses. This approach is applied to multi-degree-of-freedom (MDOF) structural models of the 3-, 9-, and 20-story steel moment resisting frames (SMRFs) of the SAC steel project (FEMA355C 2000). The analytical building models are developed using the Open System for Earthquake Engineering Simulation, OpenSees (Mazzoni et al. 2009), and were validated using the numerical data available in the literature (FEMA355C 2000; Luco 2002). Important aspects of beam strength and stiffness degradation as damage progresses during the analysis were also included in the model. To quantify the damage due the mainshock and aftershock, the buildings are first subjected to a mainshock incremental dynamic analysis and for each level of the intensity of the mainshock, the mainshock-damaged structure is then subjected to incremental dynamic analysis due to the aftershocks.

FRAMEWORK

The framework proposed for the assessment of the structural robustness of buildings is schematically presented in Figure 1. The first step of the analysis corresponds to the definition of the engineering measures considered to define failure and the thresholds used to define the performance or limit states. The following step of the analysis corresponds to the definition of the mainshock hazard. This depends on the location of the building and the foundation soil. Extensive data exists on the seismic hazard of locations in Europe, North America, and Japan (e.g., Petersen et al. 2008). From this, the mean annual rate of exceeding a ground motion intensity measure can be defined and, consequently, a probabilistic distribution of the mainshock intensity measure can be obtained. The ground motion intensity measure most used is the 5% damped linear elastic spectral acceleration at a fundamental period of the structure T_1, which is denoted as $S_a(T_1)$ (e.g. Baker 2007). Herein, the notation S will be used to refer to a spectral acceleration at a fundamental period of the structure.

Based on the definition of the hazard, a set of mainshock ground accelerograms can be defined (Step 3.1), considering either real or artificial accelerograms (e.g. Bommer and Acevedo 2004). Considering the uncertainty in the characteristics of the mainshock, several different accelerograms should be used and methods for estimating the structural response due to the mainshock

are discussed in Baker (2007), for example. When probabilistic simulation is employed, a set of mainshocks following the distribution of the spectral acceleration are used. In Step 3.2, finite element models are defined, leading at sufficient accuracy to characterize the nonlinear response to collapse, providing reliable estimates of the residual displacements and loss in stiffness and strength. Details on an example of models that can be employed to account for the strength and stiffness deterioration are described in the following section. In Step 3.3, the damage caused by the mainshock is evaluated for each of these samples. In the present paper, this is done using an incremental dynamic analysis (Vamvatsikos and Cornell 2002), but other methods for estimating the damage conditional on the mainshock ground motion intensity measure can be defined. Based on the results of these analyses, in Step 3.4, the probability of failure under mainshock alone (p_{f1}) can be estimated using:

$$p_{f1} = \int_{S^m} P(F|S^m = s^m) dP(S^m) \tag{1}$$

where S^m represent the ground motion spectral accelerations associated with the mainshock at the fundamental period of the intact structure, $P(S^m)$ corresponds to the annual probability of occurrence of a spectral acceleration associated with the mainshock, and $P(F|S^m = s^m)$ represents the probability of failure F conditional on S^m. The probabilities of exceedance of a given S^m are defined considering, for example, the data described in Petersen et al. (2008). According to Jayaram and Baker (2008) the spectral accelerations follow lognormal distributions. The term F describes a failure event, which is defined as exceedance of a limit state. When considering a collapse limit state, for example, FEMA356 (2000) reports 5% as a limiting value interstory drift ratio in buildings. It is worth noting that Eq.1 is applicable for any limit state.

Based on the properties of the mainshock, the conditional aftershock hazard can be defined in Step 4. The occurrence rate and the distribution of aftershocks have strong correlations with mainshock magnitude (Yeo and Cornell 2005). As a consequence, an aftershock hazard should be defined considering the mainshock amplitude, frequency content, and duration. Therefore, the simulation of mainshock-aftershock ought to be performed with real sequences. However, for

most sites such information in not available, and a general formulation cannot rely on existence of this data. Thus, artificial mainshock-aftershock sequences are used herein, following Luco et al. (2011), Ryu et al. (2011), and Li et al. (2012). In Step 5.1 a set of aftershock ground accelerations is defined. In Step 5.2, damage resulting from mainshock and aftershock is evaluated, following the tasks described above for the mainshock alone. The probability of failure due the aftershock conditional on the occurrence of a mainshock that does not lead to failure, p_{f2}, can be computed through:

$$p_{f2} = \frac{p_{f3} - p_{f1}}{1 - p_{f1}} \tag{2}$$

where the probability of failure considering both mainshock and aftershock, computed in Step 5.3, is given by:

$$p_{f3} = \int_{S^m} \int_{S^a} P(F|S^m = s^m, S^a = s^a) dP(S^a|S^m = s^m) dP(S^m) \tag{3}$$

and where S^a represent the ground motion spectral accelerations associated with the aftershock at the fundamental period of the intact structure, $P(S^a|S^m = s^m)$ is the conditional probability of occurrence of an aftershock with spectral acceleration S^a following a mainshock with spectral acceleration S^m, and $P(F|S^m = s^m, S^a = s^a)$ represents the probability of failure F conditional on S^m and S^a. S^a is also assumed to follow a lognormal distribution.

In Step 6, the robustness assessment is performed based on the comparison of the reliability index ($\beta = -\Phi^{-1}(p_f)$) of the undamaged structure β_{intact}, which accounts for the mainshock only, with the reliability index of the mainshock-damaged structure $\beta_{damaged}$ as (Frangopol and Curley 1987):

$$\beta_R = \frac{\beta_{intact}}{\beta_{intact} - \beta_{damaged}} \tag{4}$$

where $\beta_{intact} = -\Phi^{-1}(p_{f1})$ and $\beta_{damaged} = -\Phi^{-1}(p_{f2})$.

Herein, the reliability index for the mainshock β_{intact} is computed considering the spectral ac-

celeration event space divided in 10 intervals for ten equally likely ground motion records each denoted as earthquake E_j using a technique known as Stratified Sampling (Kiureghian 1996). The reliability index for the aftershock $\beta_{damaged}$ is computed using stratified sampling for the mainshock spectral acceleration and considering the conditional probability of failure due to aftershock as the probability of exceedance of the minimum aftershock spectral acceleration leading to failure. The probability of failure is computed considering the combination of 10 mainshock and 10 aftershock ground motion records. In this computation it is assumed herein that the mainshock and the aftershock ground motion spectral acceleration are uncorrelated.

BUILDING MODELS

General Description

The steel moment resisting frame (SMRF) buildings studied in this work are a subset of the models developed as part of the SAC Steel project (FEMA355C 2000). The buildings included in this study are a 3-, a 9-, and a 20-story buildings (denoted LA3, LA9 and LA20, respectively) which were designed for Los Angeles using pre-Northridge codes (UBC 1994). In all buildings, external frames were designed to resist the lateral seismic loads and interior frames were designed as gravity frames. As shown in Figure 2, all buildings have spans of 9.15m in both directions. The 3-story building presents no basement, while the 9- and 20-story buildings have one and two basement levels, respectively. The height of the frames is constant and equal to 3.96m, except for the first level of the two taller buildings, which have a height of 5.49m, as shown in Figure 2. A detailed description of the buildings can be found in FEMA 355C (2000) and Luco (2002).

Two-dimensional centerline models of an external frame of each of the three buildings are used for the structural analysis. According to one of the modeling alternatives presented in Luco and Cornell (2000), strong-column weak-beam ductile behavior was assumed for all structures. Brittle mechanisms and connection fracture modes were not considered.

Geometric nonlinearities are accounted for during the analysis by considering a $P-\Delta$ leaning column. A rigid diaphragm is assumed for each floor. Soil-structure interaction was not considered. Masses and loads are applied to beam-column joints. Similarly to what was defined in FEMA355C

(2000), Rayleigh damping is assigned to the models. As described in Erduran (2012), a damping ratio of 2% was assigned to the first mode and a higher mode. Following FEMA355C (2000) the higher mode considered is the fifth mode for LA20 and a mode with period 0.2s for buildings LA3 and LA9 (a period close to the LA3's 3rd modal period and the LA9's 5th modal period).

Component Modeling

The building's nonlinear behavior was modeled considering a set of four different models for each structure, as described in Table 1. The four models considered differ in the method used to simulate the beams. For the first two models, a zero-length plastic hinge element is used, considering elasto-plastic behavior with hardening and a bilinear model with deterioration (*Bilin* model in OpenSees). The third and fourth models used the same material models, but consider a finite-length plastic hinge element. In all four cases, the columns were modeled considering a distributed plasticity model and an elasto-plastic constitutive law with a 3% hardening rate assigned to each fiber. A moment-curvature section analysis showed that this corresponds to a section hardening of 3.0%, consistent with the assumptions used in the FEMA355C modeling. Thus, for the columns, the main phenomenon considered is the interaction between moment and axial load. This assumption is supported by recent testing (Newell and Uang 2008), where it is shown that columns such as the ones being modeled do not exhibit deterioration in strength by more than 10% for $P/Py \leq 0.75$ even at 8% story drift ratios. For the building under analysis, which was designed using the strong-column-weak-beam assumption, only minor deterioration in stiffness and strength of columns is expected, and disregarding these effects will have no significant impact on the results. However, for buildings consisting of slender columns, this assumption may not hold and the effect of deterioration of the strength and stiffness of the columns should be evaluated.

Zero-Length vs. Finite-Length Plastic Hinge Elements

Model idealizations for nonlinear structural analysis of beams range from phenomenological models, such as concentrated plasticity models and finite-element distributed plasticity beam-column elements, to complex continuum models based on plane-stress or solid finite-elements. In the concentrated plasticity models (Giberson 1969), nonlinear zero-length springs are discretized

at both ends of a linear-elastic beam-column element. These elements have been recently proposed as the main method for estimating seismic demands (Ibarra and Krawinkler 2005; Medina and Krawinkler 2005; Haselton and Deierlein 2007) and are the preferred modeling approach in the Applied Technology Council ATC-72 modeling guidelines proposed recently (PEER/ATC 2010). Considering that zero-length models have been widely used to model the seismic performance of buildings, in this work they are used as a reference, and the results obtained using the finite length plastic hinge elements are compared with those to ascertain their accuracy.

Scott and Fenves (2006) proposed a novel approach for modeling nonlinear behavior of frame structures based on a force-based finite-length plastic hinge beam-column elements (*beam with hinges*) which overcomes issues related to localization phenomena observed in distributed plasticity beam-column elements (Coleman and Spacone 2001). Furthermore, finite-length plastic hinge elements can model plastic hinge length explicitly and separate the behavior of beam in the span from that of beam-column connections. Compared to zero-length springs, finite-length plastic hinge elements allow faster model development due to the reduction in the number of nodes and elements.

Elasto-plastic Model with Kinematic Hardening vs. Bilinear Model With Deterioration

Steel structures are traditionally modeled considering an elasto-plastic behavior with kinematic hardening, accounting for Bauschinger effect. However, during an earthquake, structural elements are subjected to large inelastic cyclic deformations which lead to deterioration of both strength and stiffness properties of components, affecting the overall structural performance under seismic loading.

In the present work, a modified version of the Ibarra-Krawinkler (2005) phenomenological model, applicable to any force-deformation relationship, is employed to simulate beam behavior and compared to an bilinear model with kinematic hardening. This model was used by Lignos and Krawinkler (2011) to model the moment-rotation relationship of plastic hinges in steel elements. The model considers strength and stiffness deterioration, defined in terms of element geometry, material properties, and cross-section geometry.

The model by Lignos and Krawinkler (2011) defines a moment-rotation relationship and, consequently, can not be directly applied when a finite length plastic hinge is considered, which requires the use of a moment-curvature relationship. Based on the moment-rotation model described above, it is possible to define the moment-curvature $M - \chi$ model by scaling the moment-rotation backbone curve, as well as, the loading and unloading rules, in terms of the length of the plastic hinge, L_p, resulting in the model presented in Figure 3. This plastic hinge moment-rotation model is based on the assumption of a double curvature deformation, which leads to an elastic stiffness of $6EI/L$. When a finite length plastic hinge element is used, a plastic hinge length of $L_p = L/6$ should be used to recover the exact solution for the case of a fixed-fixed beam column element (Scott and Ryan 2013). All other model parameters are defined as proposed in (Lignos and Krawinkler 2011; Lignos and Krawinkler 2012). Axial and shear behavior is assumed to be linear elastic. Joint shear deformations (e.g. Gupta and Krawinkler 1999) and fracture due to low cycle fatigue (Lignos et al. 2011) are not included in this work.

For the building examples analyzed, the axial load expected to develop in beams is very low and the interaction between axial load and bending moment in beams is significantly less relevant than the deterioration of stiffness and strength which is expected to occur in the beams. For this reason, the interaction between axial load and bending moment is disregarded for the beams. The modeling assumptions made in this work are intended to provide a relatively simple structural model and, at the same time, accurately simulate the deterioration of the steel members to collapse. Thus, the modeling of some building components was neglected in these models, such as beam-column joints, column base plate connections, and partially restrained connections. The influence of these components in the robustness of steel structures to cascading events is worth studying in future works.

Model validation

The four models described were compared to those developed by Luco and Cornell (2000), also designated as *Model M1* (FEMA355C 2000), for the same buildings. The models in Luco and Cornell (2000) were developed using the software *DRAIN-2DX* (Prakash et al. 1993). The

models implemented herein were developed in OpenSees. The elements used in the *DRAIN-2DX* models correspond to concentrated plastic hinge models and a linear P-M interaction surface was assumed for compressive axial loads greater than $0.15P_y$. While the model in FEMA355C (2000) considered this simplified bilinear P-M interaction surface, the P-M interaction surface considered herein is obtained implicitly during the analysis since the columns are modeled using fiber-section nonlinear beam-column elements. A representation of the P-M interaction curve (at the section level) is presented in Figure 2(d).

The model validation performed herein includes the comparison of results for both a nonlinear static pushover and nonlinear dynamic time-history analysis. Furthermore, the buildings periods available in the literature also correlate well with the ones obtained in the FE models developed in this work, as shown in Table 2.

Nonlinear Static Analysis

The nonlinear static analyses were carried out considering the four models described in Table 1 and compared to those presented in FEMA355C (2000) and Luco (2002). The lateral load pattern applied is proportional to the first mode of vibration of each structure.

Figures 4, 5, and 6 show the pushover curves for each of the three buildings and the four finite element models used. For reference, these figures also show the design base shear quantified according to the allowable stress design method (ASD) of the 1994 Uniform Building Code (UBC 1994). It can be seen from these figures that the overall match of the pushover curve are quite good for the models with hardening . In the elastic range the differences for all models to the results presented in FEMA355C (2000) are small, increasing slightly with the increase in building height. In spite of the differences for the 20-story building being discernible in the elastic range, as shown in FEMA355C (2000), such variations are expectable as a consequence, for example, of alternative joints models. For all buildings, the models considering an elasto-plastic with hardening constitutive law (FMRH, FZLH, and FEMA355) presented a similar behavior, showing that the use of beam with hinges models does not affect significantly the results obtained. For the two taller buildings, a softening behavior is observable in all models, as a result of $P - \Delta$ effects. When the

bilinear model with deterioration is considered (FMRB and FZLB) the post peak force decreases faster, as a result of the strength deterioration considered for the beams. As a consequence of the strong-column weak-beam design, plastic hinges form firstly in the beams. The use of the bilinear model with deterioration (FMRB and FZLB) leads to a faster decrease in the post peak base-shear force, as a result of softening in the beams and corresponding change in column moment gradient, once the plastic hinges form.

In summary, the results of the pushover analysis show that the models using an elastic-plastic constitutive law lead to results similar to those described in FEMA355C (2000). Secondly, the use of zero-length and beam with hinges does not affect the results significantly, allowing the use of the finite-length plastic hinges model in subsequent analysis. Finally, the use of the bilinear model with deterioration for the beams produced larger strength reduction.

Nonlinear Dynamic Time-History Analysis

To compare the results described in Luco and Cornell (2000) with those resulting from the models used in this work, the structural response is evaluated considering forty (twenty two-component records) SAC Steel Project LA01-LA40 earthquake records. Forty nonlinear dynamic time-history response analyses were performed for each model and each of the three buildings. Obtained results were compared to those presented by Luco and Cornell (2000) in terms of maximum interstory drift ratio. The mean relative errors obtained for each model and building are presented in Table 3. For the models considering an elastic-plastic behavior (FZLH and FMRH) the results are relatively close, with a maximum mean error of 7.4%. Correlation between the floor levels where this interstory drift ratios is observed for the models developed by Luco and Cornell (2000) and the ones shown in this paper was also quite good (Ribeiro et al. 2013).

The model validation performed is considered to be sufficient for the FZLH and FMRH models. Even though no direct validation of the FZLB and FMRB models with experimental results is possible, the definition of component degradation is consistent with experimental results and P-M interaction is considered explicitly. Considering the advantages of the finite length model described and to include realistic effects of beam properties deterioration in the analysis, the FMRB model

311 is used in the subsequent analyses.

312 ANALYSIS DESCRIPTION

313 To evaluate the increased probability of failure associated with the occurrence of an aftershock
314 following a major earthquake, a simulation procedure was employed that considered as random
315 variables the spectral accelerations of the mainshock and the aftershock corresponding to the initial
316 fundamental period of the structure. Although the occurrence rate and distribution of aftershocks
317 are correlated to mainshocks magnitude (Yeo and Cornell 2005), their amplitude, frequency con-
318 tent, and duration are very difficult to simulate. Thus, artificial mainshock-aftershock sequences
319 are used herein, following Luco et al. (2011), Ryu et al. (2011), and Li et al. (2012).

320 Numerical and Computational Methods

321 The mainshock and aftershock are modeled considering a set of 10 accelerograms, each scaled
322 independently, representing different shaking intensities. For performing the incremental dynamic
323 analysis (IDA), each of the 10 mainshocks considered is scaled 10 times, by multiplying the corre-
324 spondent time-history record by the objective spectral acceleration, $S^m(T_1)$, divided by the original
325 ground motion spectral acceleration, $S^{GM}(T_1)$, corresponding to a stratified sampling of the spec-
326 tral accelerations. Each of the mainshocks can be followed by one of the 10 aftershocks. For
327 each aftershock an IDA is also performed for at least 20 intensity levels. Thus, in this analysis
328 the aftershock ground motion is incrementally scaled (by multiplying the time-history record by
329 $S^a(T_1)/S^{GM}(T_1)$), similarly to the procedure of a regular IDA, performing a number of n back-
330 to-back analysis, where n depends on the aftershock ground motion, the building being analyzed,
331 and the damage state at the end of the mainshock. Each aftershock incremental dynamic analysis
332 (AIDA) is computed considering the polarity of the aftershock (positive and negative directions).
333 A 30s time interval of free-vibration was considered between the end of the mainshock and the
334 application of the aftershock ground motion records. This duration was deemed sufficient after a
335 preliminary study that showed that the maximum nodal velocity observed during the last second
336 of this 30s interval was, for all buildings, smaller than 0.6% of the peak velocity observed for the
337 mainshock leading to highest drifts short of collapse.

For each run, the Newton-Raphson method is used for solving the nonlinear system of equations at each time step. To analyze the structure up to interstory drift ratios of 10%, a convergence study of the horizontal roof peak displacement and horizontal peak floor absolute acceleration as a function of the integration time step was performed. Time-steps considered were 0.01s, 0.005s, 0.002s, 0.001s, 0.0005s, 0.0001s, and 0.00005s. It was observed that a time step of 0.002s was sufficiently small to produce negligible errors (when compared to the 0.00005s) and no significant changes in the response were observed when smaller time steps were used.

To reduce the total computational time required for obtaining all the results for these large number of runs, an embarrassingly parallel computing framework was implemented. The implemented framework makes use of the OpenSees (v2.4.0, release 5172) sequential version and a batch-queue system called HTCondor (v7.8.0) (Thain et al. 2005). HTCondor is a specialized batch system for managing computational-intensive jobs. To make the most use of two student computer centers of Civil Engineering Departments at both Oregon State University (OSU) and Universidade Nova de Lisboa (UNL), two HTCondor pools were created, consisting of 464-cores at OSU and 96-cores at UNL. Since the research team was geographically dispersed, to minimize time needed for simulation data transfer and post-processing of the numerical results, a OSU-UNL web shared folder was created using a commercial application.

Ground Motion Records

The ground motion records used in this study were selected from the set of forty SAC Steel Project LA01-LA40 earthquake records mentioned above, considering earthquakes with the highest peak ground acceleration. These records were obtained from real and simulated ground motions, scaled so that their mean response spectrum matches the 1997 NEHRP design spectrum, as reported by Somerville et al. (1997). The time histories for Los Angeles are all derived from recordings of shallow crustal earthquakes on soil category D. The ten SAC records selected for this study are characterized by a moment magnitude M_W between 6.0 and 7.4, duration between $29.9s$ and $59.9s$, and peak ground acceleration between $0.6g$ and $1.3g$. The ten E1 to E10 ground motion records used correspond to SAC earthquakes: LA11, LA18, LA19, LA21, LA26, LA28,

LA30, LA31, LA36 and LA37.

In order to quantify the probability of failure of the structures, the spectral accelerations at Los Angeles are estimated from the hazard curves generated for the 2008 National Seismic Hazard Mapping Project (NSHMP) (Petersen et al. 2008) for soil type D. These are approximated by a log-normal distribution, under the mild assumption that the findings of Jayaram and Baker (2008) also hold for the modified ground motion records.

DETERMINISTIC NONLINEAR DYNAMIC TIME-HISTORY RESPONSE ANALYSIS

This section presents results obtained for representative nonlinear dynamic time-history response analyses, selected from those described above. The performance of the LA3 building is assessed considering a mainshock ground motion spectral acceleration of $1.2g$ and $0.9g$ for the aftershock spectral acceleration. Earthquake ground motions E1 and E4 are used as the mainshock and aftershock, respectively.

Figure 7 shows the time-history response of the LA3 building in terms of floor acceleration, roof drift ratio, and interstory drift ratio during four identified time-periods (TP1-TP4): (i) TP1 - duration of the mainshock; (ii) TP2 - free vibration period of 30s after the mainshock; (iii) TP3 - duration of the aftershock; and (iv) TP4 - free vibration period of 30s after the aftershock. This figure also shows the floor accelerations and the interstory drift ratios at the instants when peak interstory drift ratio is attained during the mainshock and the aftershock, respectively. The peak interstory drift ratio during the mainshock is 4.1% at the 3^{rd} story. In Figure 8 two moment-rotation responses are shown at two different elements. It is important to note that during the aftershock the deformations are much larger, especially for beams, whose response go beyond the peak strength, i.e. a softening response is observable.

The deformed shape of the LA3 building at the peak deformation instant is shown in Figure 9. This figure also shows the deformed shapes of the LA9 and LA20 buildings, in which, for representative analyses, the size of the circles illustrate the relative scales of rotations recorded at the end of each element. For the LA3 building, almost all beam ends had gone into the inelastic regime during the mainshock. Although the damage on the structure at the end of the mainshock is consid-

erable, as it can be inferred through the number of plastic hinges formed during the mainshock, the residual deformation is not significant (see Figure 7). At the instant when the peak interstory drift ratio is recorded during the aftershock, columns on the first story have formed plastic hinges in both ends, which indicates that an undesirable soft story mechanism is formed. Four plastic hinges have also formed in second story columns and two in the third one. Effects of higher modes in the instants where peak interstory drifts are recorded can be observed in the LA9 and LA20 building response especially during the aftershock (see Figure 9).

AFTERSHOCK INCREMENTAL DYNAMIC ANALYSIS

For each mainshock-aftershock combination and each mainshock intensity, an aftershock incremental dynamic analysis (AIDA), for increasing aftershock intensities, is performed in order to compute the failure probability under this sequence of events. In Figure 10, AIDA curves are shown for four mainshock ground motion spectral accelerations. For sake of brevity only results from the LA3 building are shown herein. Earthquake E5 is considered as mainshock. Ten AIDA curves are then computed for the ten possible aftershocks. For each mainshock intensity, the results obtained show the variation of the peak interstory drift ratio, θ_{max}, as a function of the aftershock ground motion spectral acceleration.

The value of 10% of interstory drift ratio is considered to be the threshold for failure (Baker 2007). Higher values of interstory drift ratio will lead to violation of the performance threshold and thus be considered as failure. Previous probability-based studies (e.g., Baker 2007) have concluded that 10% IDR is an adequate threshold to define collapse in a numerical framework. Although FEMA356 (2000) defines 5% IDR for collapse prevention, to study the structural robustness (i.e., the capacity of the structure to sustain damage) this larger value allows for the assessment of the nonlinear structural behavior under very large deformations, which contributes to the accurate evaluation of the reliability-based structural robustness by allowing for more accurate computation of the probability of failure.

Figure 10 shows the AIDA curves illustrating the decrease in capacity with the increase in the mainshock intensity. For example, the aftershock E4 ground motion spectral acceleration that

leads the structure to failure is $1.7g$ when the mainshock ground motion spectral acceleration is $1.2g$, whereas when the mainshock ground motion spectral acceleration is $2.4g$ the aftershock spectral acceleration that leads to failure is $1.1g$.

ROBUSTNESS ASSESSMENT RESULTS

Figure 11 shows the lowest aftershock spectral acceleration that leads the LA3 building to fail ($\theta_{max} = 10\%$) versus the mainshock spectral acceleration. The figure corresponds to results obtained using earthquake E_5 for both the mainshock and the aftershock. It can be seen that for lower intensities of the mainshock there is little impact of mainshock on the aftershock spectral acceleration that leads to failure. Additionally, for increasing mainshock intensities, the aftershock spectral accelerations that lead to failure are reduced, since the mainshock induced damage reduces the capacity of the structure to sustain additional damage due to the aftershocks. Since the same accelerograms are used for generating both mainshock and aftershock, application of a mainshock only or an aftershock following a low intensity mainshock (i.e., causing no damage to the structure) are equivalent. Consequently, the lowest mainshock spectral acceleration leading to failure is identical to the (minimum) aftershock spectral acceleration which leads to failure for very low mainshock intensities.

In Figure 12 the median aftershock ground motion spectral acceleration that leads the structures to failure is represented as a function of the median mainshock ground motion spectral acceleration. A similar trend to that described for Figure 11 is observable here, but now for the entire set of AIDA analyses considered. Figure 12 also shows the median residual displacements after application of the mainshock. The results show a significant correlation between the increase in residual displacements and the reduction in the aftershock leading to failure, indicating that residual displacements could be used as a measure of damage.

In Table 4, the probabilities of failure and the corresponding reliability indices are presented considering mainshock, aftershock and mainshock+aftershock. The redundancy indicator, β_r, introduced by Frangopol and Curley (1987) is used to compare robustness of the three buildings. The reliability indices obtained considering only the mainshock are very similar across structures,

showing that the design procedure applied is consistent. However, the probability of failure considering aftershock and mainshock-induced damage increases much more significantly for buildings LA3 and LA20, than for LA9.

The results obtained for the redundancy index, β_r, show that LA9, although less safe than LA3 and LA20 under a mainshock alone, is significantly more robust. These results can be correlated to the LA9 building ability to distribute damage over its entire height of the building as shown in Figure 9.

CONCLUSIONS

In this paper, a reliability-based robustness assessment methodology for steel moment resisting frame structures subjected to post-mainshock seismic events was proposed and exemplified. Robustness is computed through comparison of the structural reliability index under a mainshock, considering the undamaged structure, and under an aftershock applied to the mainshock-damaged structure. Probabilities of failure are computed through simulation, using nonlinear finite element models that explicitly reproduce damage induced by strong shaking. The methodology is exemplified using back-to-back mainshock-aftershock nonlinear dynamic time-history analyses.

For structures expected to form strong-column weak-beam failure mechanisms, a finite element modeling approach was presented in which columns were modeled using force-based fiber-section distributed plasticity elements and beams were modeled using a recently proposed phenomenological bilinear model with deterioration. The models used for the columns directly account for axial load- bending moment interaction. For the beams, the deterioration behavior defined for the plastic hinges is fundamental for accurate performance assessments under mainshock-aftershock sequences. The finite-length plastic hinge element is used due to its ability to model plastic hinge lengths explicitly and to separate the behavior of beam in the span from that of beam-column connections.

Two-dimensional models of a 3-, 9-, and 20-story steel buildings, designed for the SAC project for Los Angeles, California, were implemented in the OpenSees framework. For simulating the mainshock-aftershock sequence of events, ten different mainshock and aftershock ground motion

records were combined. The spectral accelerations at fundamental periods of the buildings were used to simulate mainshock and aftershock intensities that follow lognormal distributions. "Back-to-back" mainshock-aftershock incremental dynamic analyses are performed for each combination of mainshock-aftershock, while failure is defined in terms of the exceedance of an interstory drift threshold. It is worth noting that the results presented here are sensitive to the frequency content of the ground motions (both aftershock and mainshock), period elongation due to cyclic deterioration in stiffness from the mainshock, and the definition of the fundamental period of the frame structures. These important factors are not considered herein, and as discussed in Faggella et al. (2013) can only be adequately accounted for by using a vector-valued ground motion intensity measure. The use of vector-valued ground motion intensity measures falls outside the scope of this paper.

Application of the reliability-based robustness assessment showed the importance of considering the aftershock in the evaluation of safety of structures under seismic events, as a significant increase in failure probability was observed when mainshock-aftershock sequences were considered. Moreover, this study showed that the LA9 building, although initially more susceptible to failure than the LA3 and LA20 buildings, presented significantly higher robustness for the aftershock events ($\beta_r = 41.52$ for LA9 versus $\beta_r = 19.32$ and $\beta_r = 11.31$ for LA3 and LA20, respectively). In fact, robustness is defined in terms of the increase in probability of failure considering damage, and LA9, although less safe than LA3 and LA20 under a mainshock alone, presents a lower reduction in reliability index when cascading events are considered. Thus, it can also be concluded that the probabilities of failure for multiple hazards requires explicit modeling of the hazards and simulation methods need to accurately model the damage induced by the cascading hazards.

ACKNOWLEDGEMENTS

In the development of this research work, the first and third author would like to acknowledge the support of the Portuguese Science and Technology Foundation through the fellowship SFRH/BD/77722/2011 and UNIC Research Center at the New University of Lisbon. The support of the School of Civil and Construction Engineering at Oregon State University to the second au-

thor is gratefully acknowledged. The first author would also like to acknowledge the support of Oregon State University during the period in which he was a visiting Ph.D. student. The support of the Nottingham Transportation Engineering Center to the third author is gratefully acknowledged. The opinions and conclusions presented in this paper are those of the authors and do not necessarily reflect the views of the sponsoring organizations.

References

Baker, J., Schubert, M., and Faber, M. (2008). "On the assessment of robustness." *Structural Safety*, 30(3), 253–267.

Baker, J. W. (2007). "Probabilistic structural response assessment using vector-valued intensity measures." *Earthquake Engineering and Structural Dynamics*, 36(13).

Bommer, J. J. and Acevedo, A. B. (2004). "The use of real earthquake accelerograms as input to dynamic analysis." *Journal of Earthquake Engineering*, 8(spec01), 43–91.

Cavaco, E., Casas, J., Neves, L., and Huespe, A. (2013). "Robustness of corroded reinforced concrete structures: a structural performance approach." *Structure and Infrastructure Engineering*, 9(1), 42–58.

Coleman, J. and Spacone, E. (2001). "Localization issues in force-based frame elements." *ASCE Journal of Structural Engineering*, 127(11), 1257–1265.

Erduran, E. (2012). "Evaluation of rayleigh damping and its influence on engineering demand parameter estimates." *Earthquake Engineering & Structural Dynamics*, 41(14), 1905–1919.

Faggella, M., Barbosa, A. R., Conte, J. P., Spacone, E., and Restrepo, J. I. (2013). "Probabilistic seismic response analysis of a 3-d reinforced concrete building." *Structural Safety*, 44, 11–27.

FEMA355C (2000). *State of the Art Report on Systems Performance of Steel Moment Frames Subjecte to Earthquake Ground Shaking*. SAC Joint Venture for the Federal Emergency Management Agency, Washington, DC.

FEMA356 (2000). "Prestandard and commentary for the seismic rehabilitation of buildings: FEMA-356.

526 Fragiacomo, M., Amadio, C., and Macorini, L. (2004). "Seismic response of steel frames under
527 repeated earthquake." *Engineering Structures*, 26(13), 2021–2035.
528 Frangopol, D. and Curley, J. (1987). "Effects of damage and redundancy on structural reliability."
529 *ASCE Journal of Structural Engineering*, 113(7), 1533–1549.
530 Giberson, M. (1969). "Two nonlinear beams with definitions of ductility." *Journal of the Structural*
531 *Division*, 95(2), 137–157.
532 Gupta, A. and Krawinkler, H. (1999). "Seismic demands for performance evaluation of steel mo-
533 ment resisting frame structures." *Report No. 132*, The John A. Blume Earthquake Engineering
534 Center.
535 Haselton, C. and Deierlein, G. (2007). "Assessomg seismic collapse safety of modern reinforced
536 concrete frame buildings." *Report No. 156*, The John A. Blume Earthquake Engineering Center,
537 Stanford University.
538 Ibarra, L. F. and Krawinkler, H. (2005). "Global collapse of frame structures under seismic exci-
539 tations." *Report No. 152*, The John A. Blume Earthquake Engineering Research Center, Depart-
540 ment of Civil Engineering, Stanford University, Stanford, CA.
541 Jayaram, N. and Baker, J. (2008). "Statistical tests of the joint distribution of spectral acceleration
542 values." *Bulletin of the Seismological Society of America 2008*, 98(5), 2231–2243.
543 Kiureghian, A. D. (1996). "Structural reliability methods for seismic safety assessment: a review."
544 *Engineering Structures*, 18(6), 412 – 424.
545 Lee, K. and Foutch, D. (2004). "Performance evaluation of damaged steel frame buildings sub-
546 jected to seismic loads." *ASCE Journal of Structural Engineering*, 130(4), 588–599.
547 Li, Q. and Ellingwood, B. R. (2007). "Performance evaluation and damage assessment of steel
548 frame buildings under main shock-aftershock earthquake sequences." *Earthquake Engineering*
549 *& Structural Dynamics*, 36(3), 405–427.
550 Li, Y., Song, R., van de Lindt, J., Nazari, N., and Luco, N. (2012). "Assessment of wood and steel
551 structures subjected to earthquake mainshock-aftershock." *XV World Conference on Earthquake*
552 *Engineering*, Lisbon, Portugak.

553 Lignos, D. and Krawinkler, H. (2012). "Development and utilization of structural component
554 databases for performance-based earthquake engineering." *ASCE Journal of Structural Engi-*
555 *neering*.

556 Lignos, D. G., Chung, Y., Nagae, T., and Nakashima, M. (2011). "Numerical and experimen-
557 tal evaluation of seismic capacity of high-rise steel buildings subjected to long duration earth-
558 quakes." *Comput. Struct.*, 89(11-12), 959–967.

559 Lignos, D. G. and Krawinkler, H. (2011). "Deterioration modeling of steel components in sup-
560 port of collapse prediction of steel moment frames under earthquake loading." *ASCE Journal of*
561 *Structural Engineering*, 137(11), 1291–1302.

562 Lind, N. C. (1995). "A measure of vulnerability and damage tolerance." *Reliability Engineering*
563 *and System Safety*, 48(1), 1–6.

564 Luco, N. (2002). "Probabilistic seismic demand analysis, SMRF connection fractures, and near-
565 source effects." Ph.D. thesis, Department of Civil and Environmental Engineering, Stanford
566 University, Stanford, California.

567 Luco, N., Bazzurro, P., and Cornell, C. (2004). "Dynamic versus static computation of the residual
568 capacity of a mainshock-damaged building to withstand an aftershock." *13th World Conference*
569 *on Earthquake Engineering*, Vancouver, Canada.

570 Luco, N. and Cornell, C. A. (2000). "Effects of connection fractures on smrf seismic drift de-
571 mands." *ASCE Journal of Structural Engineering*, 126(1), 127–136.

572 Luco, N., Gerstenberger, M. C., Uma, S., Ryu, H., Liel, A. B., and Raghunandan, M. (2011).
573 "A methodology for post-mainshock probabilistic assessment of building collapse risk." *Pacific*
574 *Conference on Earthquake Engineering*, Auckland, New Zealand (April).

575 Mazzoni, S., McKenna, F., Scott, M. H., and Fenves, G. L. (2009). *The OpenSees command lan-*
576 *guage manual, Version 2.0*. Pacific Earthquake Eng. Research Center, Univ. California at Berke-
577 ley.

578 Medina, R. and Krawinkler, H. (2005). "Evaluation of drift demands for the seismic performance
579 assessment of frames." *ASCE Journal of Structural Engineering*, 131(7), 1003–1013.

Newell, J. D. and Uang, C.-M. (2008). "Cyclic behavior of steel wide-flange columns subjected to large drift." *Journal of structural engineering*, 134(8), 1334–1342.

Newmark, N. and Rosenbleuth, E. (1971). *Fundamental of Earthquake Engineering*. Prentice-Hall.

PEER/ATC (2010). "Modeling and acceptance criteria for seismic design and analysis of tall buildings." *Report No. 72-1*, ATC - Applied Techonology Council.

Petersen, M., Frankel, A., Harmsen, S., Mueller, C., Haller, K., Wheeler, R., Wesson, R., Zeng, Y., Boyd, O., Perkins, D., Luco, N., Field, E.H. Wills, C., and Rukstales, K. (2008). "Documentation for the 2008 update of the united states national seismic hazard maps." *Report no.*, U.S. Geological Survey Open-File Report 2008-1128. 61 p.

Prakash, V., Powell, G., and Campbell, S. (1993). "Drain-2dx base program description and user guide, version 1.0." *Report No. UCB/SEMM-93/17-18*, Engineering Mechanics and Material, Department of Civil Engineering, University of California, Berkeley, CA.

Ribeiro, F., Barbosa, A., and Neves, L. (2013). *Numerical analysis of steel moment resisting frames under seismic ground motions*.

Ruiz-García, J. (2012). "Mainshock-aftershock ground motion features and their influence in building's seismic response." *Journal of Earthquake Engineering*, 16(5), 719–737.

Ryu, H., Luco, N., Uma, S., and Liel, A. (2011). "Developing fragilities for mainshock-damaged structures through incremental dynamic analysis." *Pacific Conference on Earthquake Engineering*, Auckland, New Zealand (April).

Scott, M. and Ryan, K. (2013). "Moment-rotation behavior of force-based plastic hinge elements." *Earthquake Spectra*, 29(1).

Scott, M. H. and Fenves, G. L. (2006). "Plastic hinge integration methods for force-based beam-column elements." *ASCE Journal of Structural Engineering*, 132(2), 244–252.

Somerville, P., Smith, N., Punyamurthula, S., and Sun, J. (1997). "Development of ground motion time histories for phase ii of the fema/sac steel project." *Report No. SAC/BD-97/04*, SAC Background Document.

Starossek, U. (2006). "Progressive collapse of structures: Nomenclature and procedures." *Struc-*

607 *tural Engineering International*, 2(16), 113–117.

608 Starossek, U. and Haberland, M. (2008). “Measures of structural robustness–requirements and
609 applications.” *ASCE SEI Structures Congress - Crossing Borders*, Vancouver, Canada.

610 Thain, D., Tannenbaum, T., and Livny, M. (2005). “Distributed computing in practice: the condor
611 experience..” *Concurrency - Practice and Experience*, 17(2-4), 323–356.

612 UBC (1994). *"Structural Engineering Design Provisions", Uniform Building Code, Vol. 2*. Inter-
613 national Conference of Building Officials.

614 Vamvatsikos, D. and Cornell, C. (2002). “Incremental dynamic analysis.” *Earthquake Engineering*
615 *and Structural Dynamics*, 31(3), 491–514.

616 Yeo, G. L. and Cornell, C. (2005). “Stochastic characterization and decision bases under time-
617 dependent aftershock risk in performance-based earthquake engineering.” *Report no.*, Pacific
618 Earthquake Engineering Research Center - College of Engineering. PEER Report 2005/13.

List of Tables

Table 1. Models description

Model	Columns		Beams	
	Element formulation	Material	Element formulation	Material
FZLH	**F**orce-based fiber-section distributed plasticity	Elasto-plastic with hardening	**Z**ero-**l**ength (Concentrated plasticity)	Elasto-plastic with **H**ardening
FZLB				**B**ilinear with deterioration (*Bilin*)
FMRH			Finite-length plastic hinge (**M**odified-**R**adau)	Elasto-plastic with **H**ardening
FMRB				**B**ilinear with deterioration (*Bilin*)

Table 2. Periods of vibration for OpenSees models and FEMA355C model

	LA3 Building		LA9 Building		LA20 Building	
	OpenSees	FEMA355C	OpenSees	FEMA355C	OpenSees	FEMA355C
1^{st} Mode	1.04s	1.03s	2.40s	2.34s	4.10s	3.98s
2^{nd} Mode	0.34s	0.33s	0.90s	0.88s	1.40s	1.36s
3^{rd} Mode	0.18s	0.17s	0.52s	0.50s	0.81s	0.79s

Table 3. Mean relative difference in peak interstory drift ratio to model M1 (FEMA355C 2000)

Building	Model			
	FZLH	FMRH	FMRB	FZLB
LA3	4.6%	4.0%	5.6%	8.7%
LA9	4.5%	5.1%	6.4%	8.4%
LA20	7.4%	6.3%	9.3%	9.8%

Table 4. Probabilities of failure, reliability indexes and redundancy index associated with the scenarios considered

Scenario		LA3 Building	LA9 Building	LA20 Building
Mainshock	Probability of failure (p_{f1})	3.56×10^{-4}	7.22×10^{-4}	6.17×10^{-4}
	Reliability index (β)	3.38	3.19	3.23
Mainshock $\bigcup$ Aftershock	Probability of failure (p_{f3})	1.02×10^{-3}	1.66×10^{-3}	2.23×10^{-3}
	Reliability index (β)	3.08	2.94	2.84
Aftershock | Mainshock	Probability of failure (p_{f2})	6.64×10^{-4}	9.39×10^{-4}	1.61×10^{-3}
	Reliability index (β)	3.21	3.11	2.95
Redundancy index β_r		19.32	41.52	11.31

List of Figures

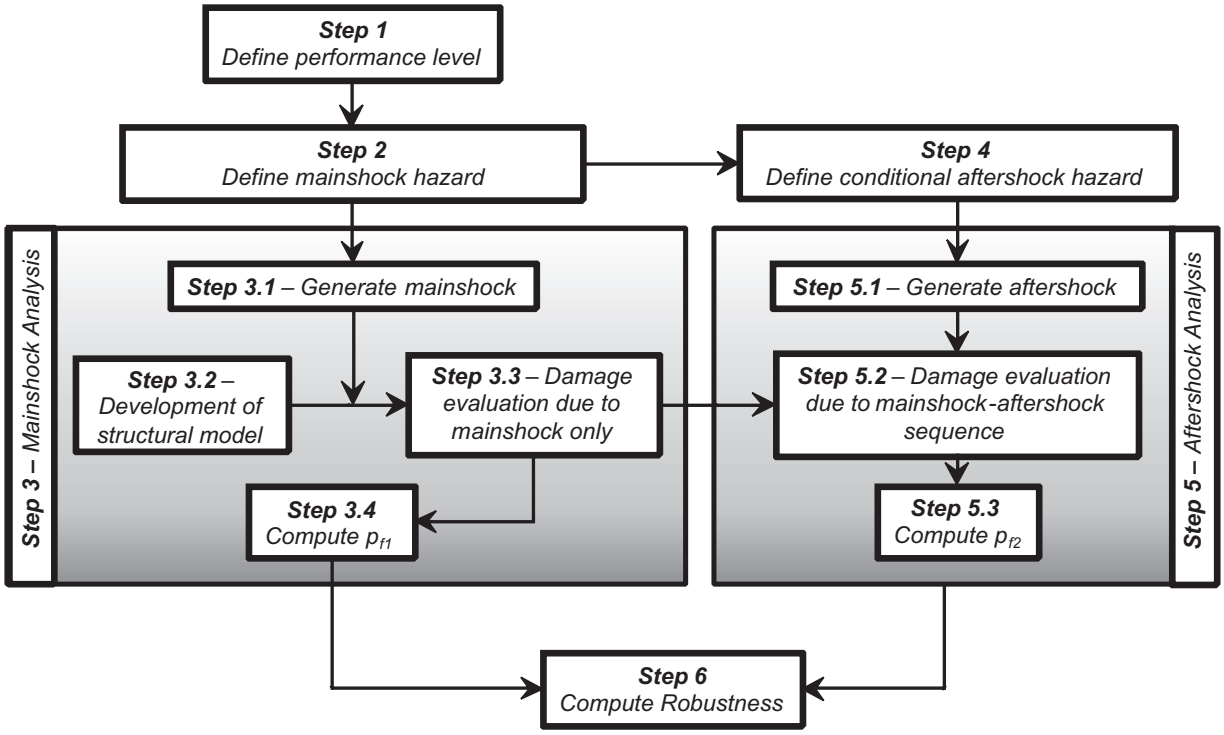

Figure 1. Flowchart for the robustness assessment of buildings subjected to cascading seismic events

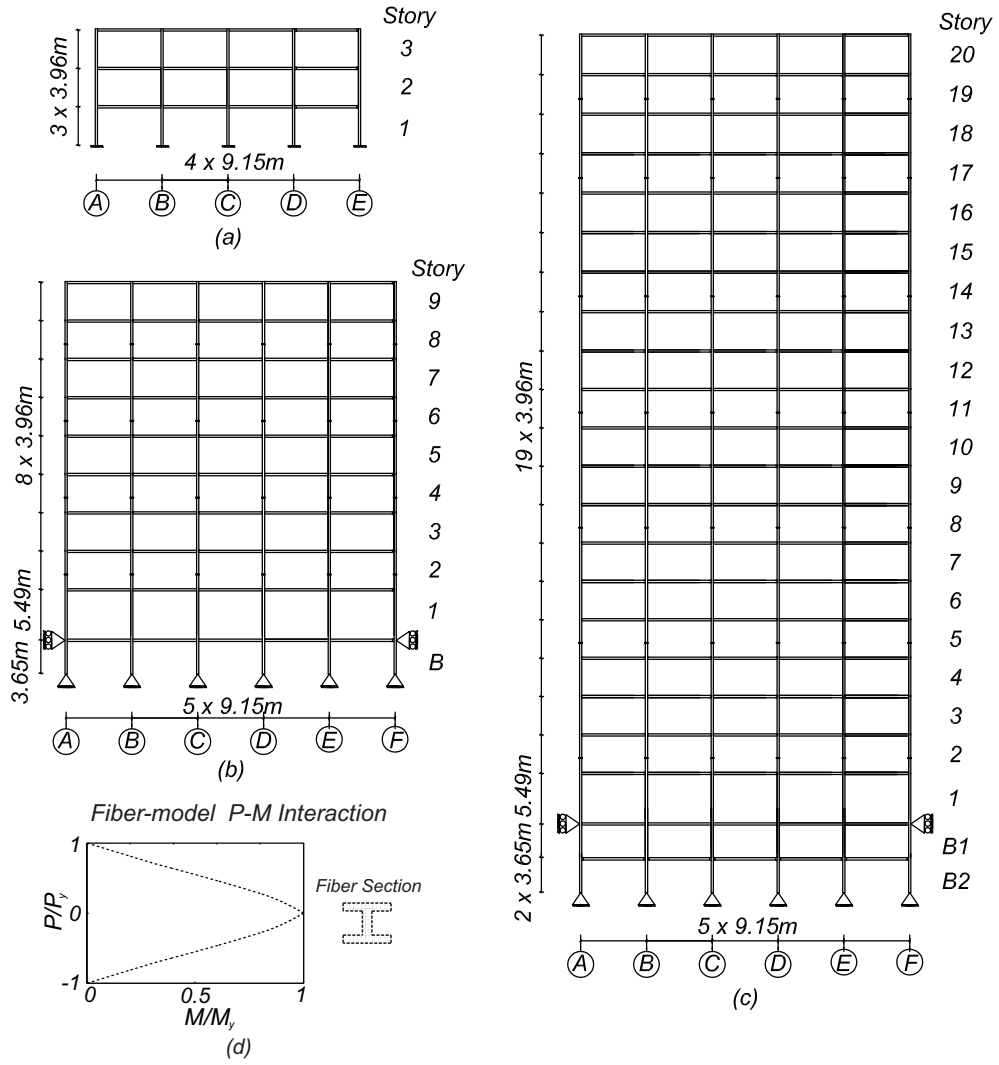

Figure 2. Building Models (a) LA3; (b) LA9 and (c) LA20 and (d) P-M interaction curve

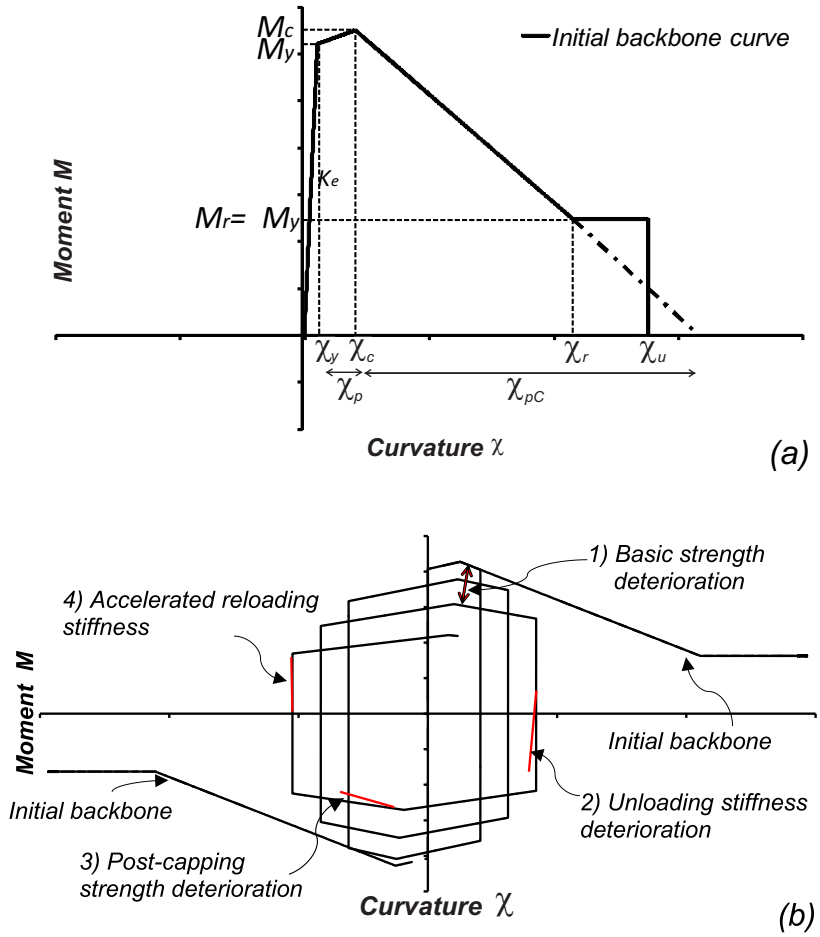

Figure 3. Adapted modified Ibarra-Krawinkler model: (a) backbone curve; and (b) basic modes of cyclic deterioration

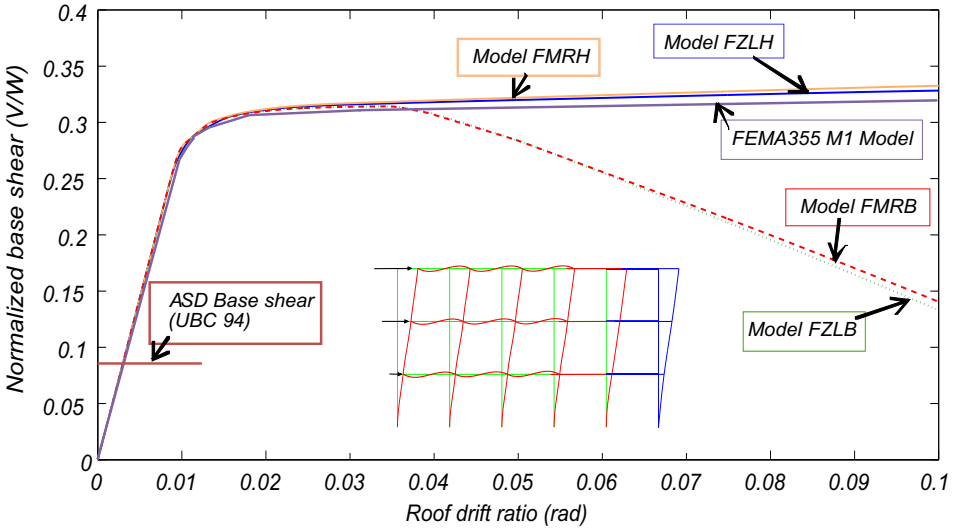

Figure 4. LA3 building - Nonlinear static (pushover) capacity curve considering a 1^{st} mode lateral load pattern

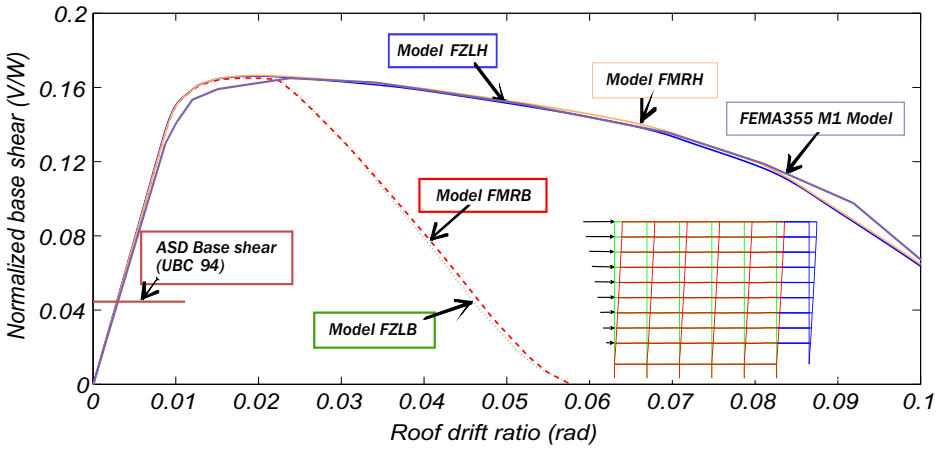

Figure 5. LA9 building - Nonlinear static (pushover) capacity curve considering a 1^{st} mode lateral load pattern

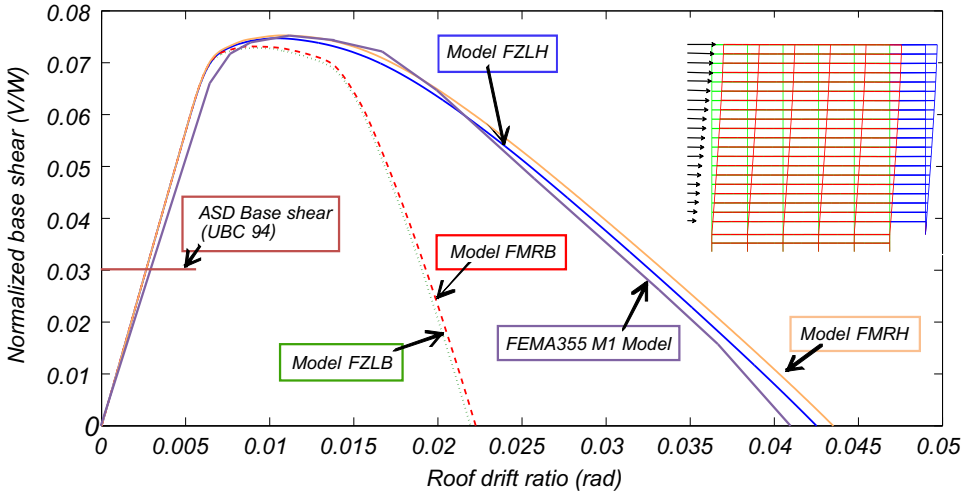

Figure 6. LA20 building - Nonlinear static (pushover) capacity curve considering a 1^{st} mode lateral load pattern

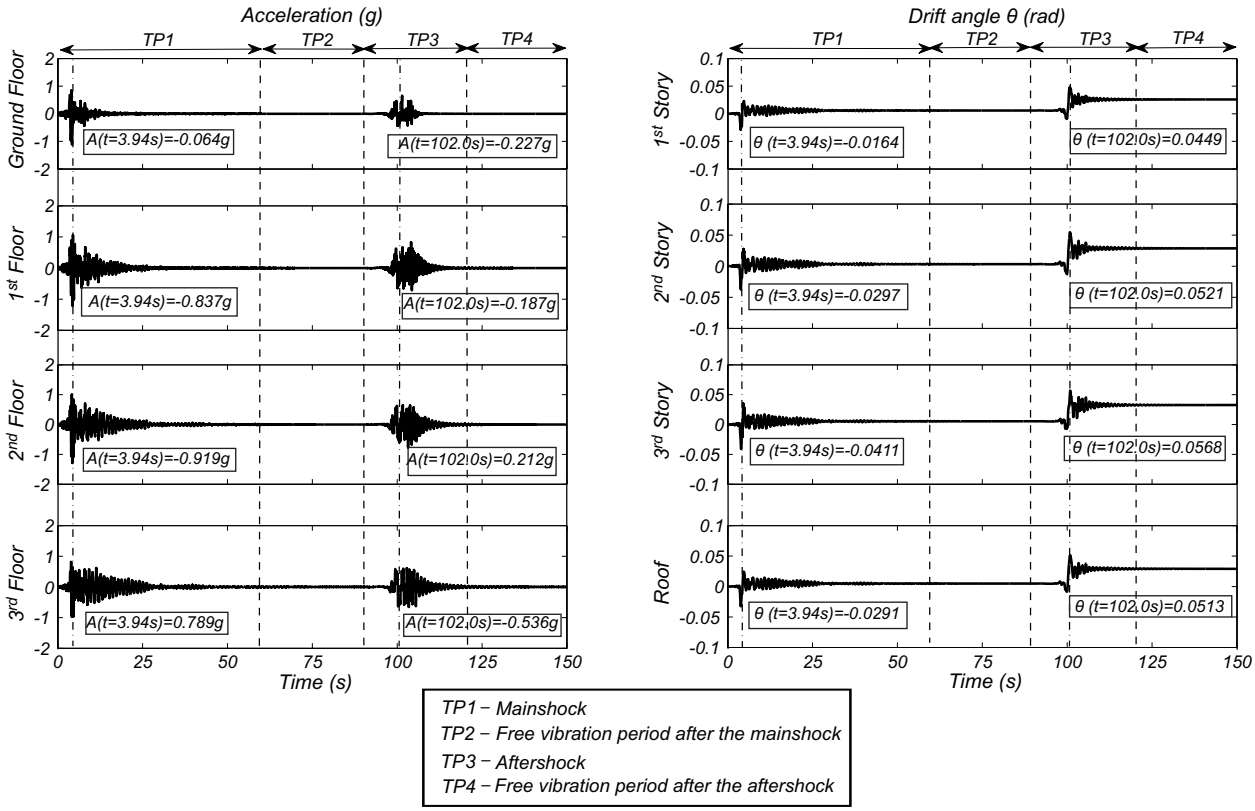

Figure 7. LA3 building - Example of a mainshock-aftershock back-to-back acceleration and drift response time-histories

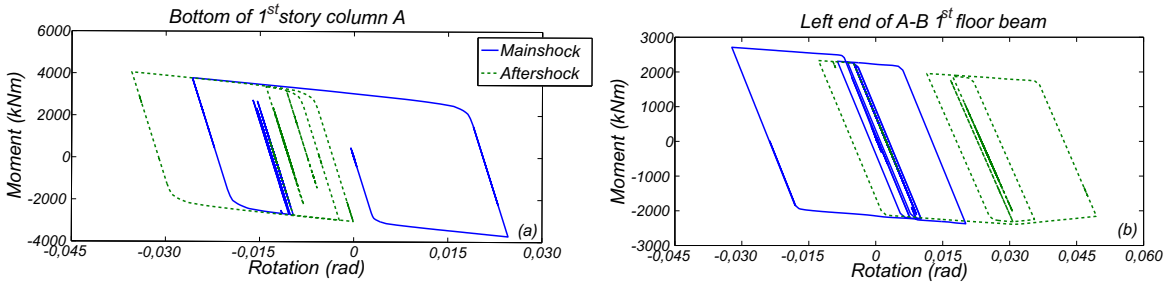

Figure 8. LA3 building hinge moment-rotation response at: (a) bottom of first story in grid line A; (b) left end of first floor level beam A-B

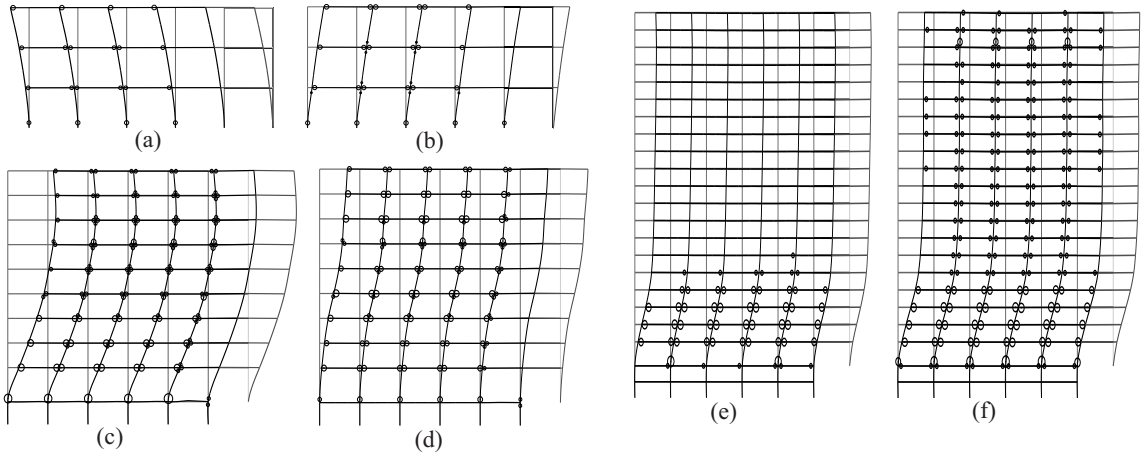

Figure 9. Deformed shapes of the buildings at two different instants: (a,c,d) - Peak interstory drift ratio during the mainshock; and (b,d,f) - Peak interstory drift ratio during the aftershock, for LA3, LA9 and LA20, respectively.

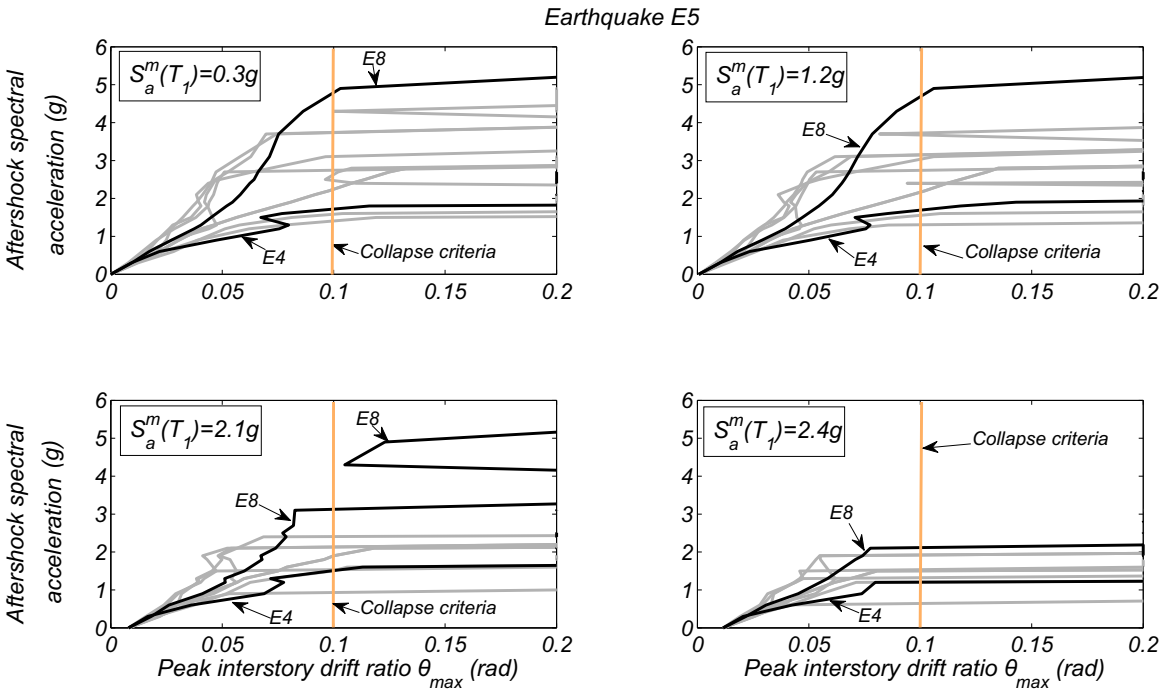

Figure 10. LA3 building - Aftershock IDA curves for ten earthquake records and four different mainshock ground motion spectral accelerations

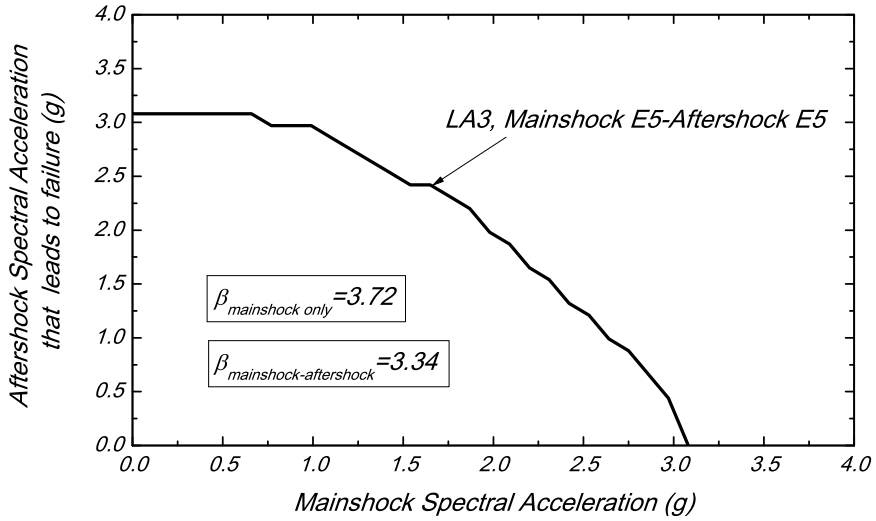

Figure 11. LA3 building - Aftershock ground motion spectral acceleration at the fundamental period of the intact structure that leads to failure as a function of the mainshock ground motion spectral acceleration for earthquake E5

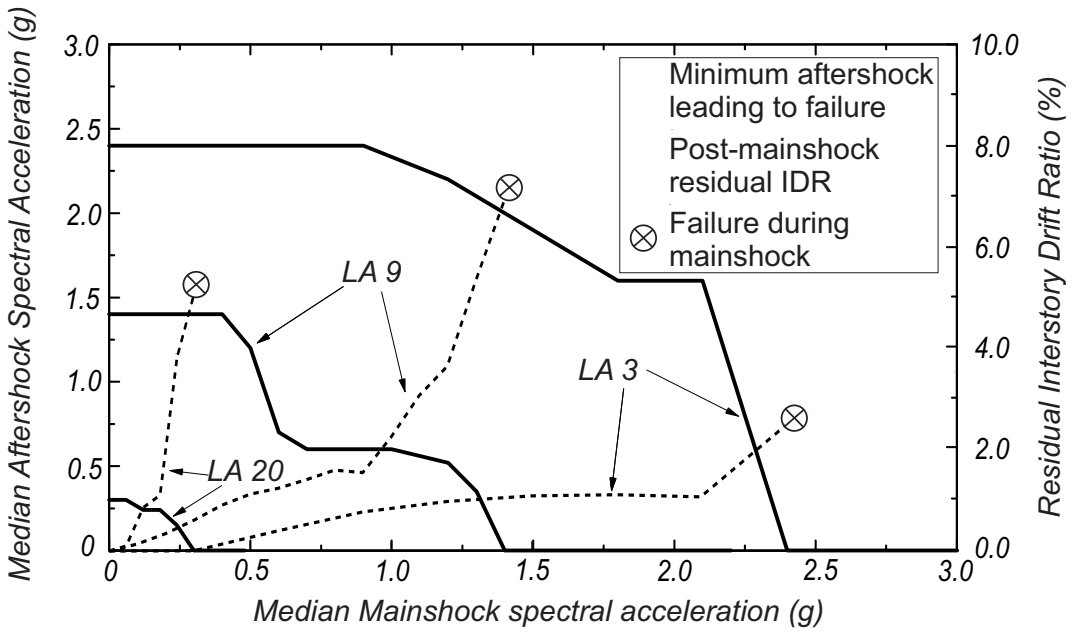

Figure 12. Median lowest aftershock ground motion spectral acceleration at the fundamental period of the intact structure that leads to failure (solid line and left vertical axis) and median residual interstory drift ratio after mainshock (dashed line and left vertical axis) as a function of the median mainshock ground motion spectral acceleration